Self-oscillations in a cascaded Raman laser made with a highly nonlinear photonic crystal fiber

P. Suret[1], **N. Y. Joly**[1], **G. Mélin**[2], **and S. Randoux**[1]

[1] *Laboratoire de Physique des Lasers, Atomes et Molécules, UMR CNRS 8523, Centre d' Etudes et de Recherches Lasers et Applications, Université des Sciences et Technologies de Lille, F-59655 Villeneuve d'Ascq, France*

[2] *Draka, route de Nozay, 91460 Marcoussis, France*

stephane.randoux@univ-lille1.fr

Abstract: We report the observation of self-oscillations of the output power in a cascaded Raman fiber laser delivering two Stokes components. Our cascaded Raman fiber laser is made with a highly nonlinear photonic crystal fiber and it oscillates within a Perot-Fabry cavity formed by weak Fresnel reflections from the fiber ends. From our experimental and theoretical study, we identify stimulated Raman scattering as being the physical effect dominant in the emergence of unstable behaviors inside the Perot-Fabry cavity. Mechanisms of laser destabilization are thus found to be very different from polarization mechanisms previously identified as being responsible for unstable behaviors in conventional one-stage Raman fiber lasers [14, 15].

OCIS codes: (140.3550) Lasers, Raman; (140.3510) Lasers, fiber; (160.2290) Fiber materials; (190.3100) Instabilities and chaos.

References and links

1. E. M. Dianov, I. A. Bufetov, M. M. Bubnov, M. V. Grekov, S. A. Vasiliev, and O. I. Medvedkov, "Three-cascaded 1407-nm Raman laser based on phosphorus-doped silica fiber," Opt. Lett. **25,** 402–404 (2000).
2. M. D. Mermelstein, J.-C. Bouteiller, P. Steinvurzel, C. Horn, K. Feder, and B. Eggleton, "Configurable three-wavelength Raman fiber laser for Raman amplification and dynamic gain flattening," IEEE. Photon. Technol. Lett. **13,** 1286–1288 (2001).
3. Y. Han, C. Kim, J. I. Kang, U. Paek, and Y. Chung, "Multiwavelength Raman fiber-ring laser based on tunable cascaded long-period gratings," IEEE. Photon. Technol. Lett. **15,** 383–385 (2003).
4. Y. Zhao and S. D. Jackson, "Highly efficient free running cascaded Raman fiber laser that uses broadband pumping," Opt. Express **13,** 4731–4736 (2005).
5. S. Cierullies, H. Renner, and E. Brinkmeyer, "Numerical optimization of multi-wavelength and cascaded Raman fiber lasers," Opt. Commun. **217,** 233–238 (2003).
6. C. Huang, Z. Cai, C. Ye, H. Xu, and Z. Luo, "Optimization of dual-wavelength cascaded Raman fiber lasers using an analytic approach," Opt. Commun. **272,** 414–419 (2007).
7. I. A. Bufetov and E. M. Dianov, "A simple analytic model of a cw multicascade fibre Raman laser," Quantum Electron. **30,** 873–877 (2000).
8. F. Leplingard, C. Martinelli, S. Borne, L. Lorcy, D. Bayart, F. Castella, P. Chartier, and E. Faou, "Modeling of multiwavelength Raman fiber lasers using a new and fast algorithm," IEEE Photon. Technol. Lett. **16,** 2601–2603 (2004).
9. M. Rini, I. Cristiani, and V. Degiorgio, "Numerical Modeling and Optimization of Cascaded CW Raman Fiber Lasers," IEEE J. Quantum Electron. **36,** 1117–1122 (2000).
10. B. Burgoyne, N. Godbout, and S. Lacroix, "Theoretical analysis of *n*th-order cascaded continuous-wave Raman fiber lasers. II. Optimization and design rules," J. Opt. Soc. Am. B **22,** 772–776 (2005).

#94134 - $15.00 USD Received 20 Mar 2008; revised 5 May 2008; accepted 6 May 2008; published 11 Jul 2008

11. B. Burgoyne, N. Godbout, and S. Lacroix, "Transient regime in a *n*th-order cascaded CW Raman fiber laser," Opt. Express **12,** 1019–1024 (2004).
12. S. D. Jackson and P. H. Muir "Theory and numerical simulation of nth-order cascaded Raman fiber lasers," J. Opt. Soc. Am. B **18,** 1297–1306 (2001).
13. S. A. Babin, D. V. Churkin, A. A. Fotiadi, S. I. Kablukov, O. I. Medvedkov, and E. V. Podivilov, "Relative Intensity Noise in Cascaded Raman Fiber Lasers," IEEE Photon. Technol. Lett. **17,** 2553–2555 (2005).
14. A. Doutté, P. Suret, and S. Randoux, "Influence of light polarization on dynamics of continuous-wave-pumped Raman fiber lasers," Opt. Lett. **28,** 2464–2466 (2003).
15. P. Suret, A. Doutté, and S. Randoux, "Influence of light polarization on dynamics of all-fiber Raman lasers: theoretical analysis," Opt. Lett. **29,** 2166–2168 (2004).
16. S. Randoux, A. Doutté, and P. Suret, "Polarization-resolved analysis of the characteristics of a Raman laser made with a polarization maintaining fiber," Opt. Commun. **260,** 232–241 (2006).
17. S. Randoux, N. Y. Joly, G. Mélin, A. Fleureau, L. Galkovsky, S. Lempereur, and P. Suret, "Grating-free Raman laser using highly nonlinear photonic crystal fiber" Opt. Express **15,** 16035–16043 (2007).
18. S. Randoux, V. Lecoeuche, B. Ségard, and J. Zemmouri, "Dynamical behavior of a Brillouin fiber ring laser emitting two Stokes components" Phys. Rev. A **52,** 2327–2334 (1995).
19. V. Babin, A. Mocofanescu, V. I. Vlad, and M. J. Damzen, "Analytical treatment of laser-pulse compression in stimulated Brillouin scattering" J. Opt. Soc. Am. B **16,** 155–163 (1999).

1. Introduction

Cascaded Raman fiber lasers (RFLs) are light sources which can be currently designed to deliver customized spectral lines across the $1-1.8$ μm wavelength region. Multi-wavelength lasing via cascaded Raman scattering has been achieved in a variety of configurations, including various kind of fibers and various cavity geometries [1, 2, 3, 4]. Optimization of threshold power and efficiency of cascaded RFLs is a problem which has recently received great attention and extensive literature can be found about this topic [5, 6, 7, 8, 9, 10]. Taking models governing the longitudinal evolutions of total optical powers carried by multiple Stokes and pump components at steady state, many authors have developed analytical or numerical methods to determine and to optimize the power delivered by cascaded RFLs at some wavelength of interest [5, 6, 7, 8, 9, 10].

On the other hand, the question of time-dependent behaviors of cascaded RFLs is a subject which has received much less attention. Dynamical behavior of cascaded RFLs has been studied in ref. [11] by examining the transient response of nth-order cascaded RFLs to abrupt switches of the pump power. It has been shown that the RFL stable steady-state is reached after transient power spikes lasting typically a few tens of cavity round trip times (i.e. a few tens of μs). A theoretical study of the response of cascaded RFLs to a slow sinusoidal modulation of the pump power (i.e. much slower than the cavity round trip time of ~ 10 μs) has demonstrated the occurrence of a slow antiphase dynamics between Stokes modes [12]. Finally noise properties of cascaded RFLs, which are of importance in lightwave transmission systems, have also been examined in a two-stage RFL by considering transfer of relative intensity noise from pump to Stokes components [13]. To the best of our knowledge, self-oscillations of the Stokes optical power have been reported only in cw-pumped RFLs delivering a single Stokes component [14]. It has been shown that they arise from linear and nonlinear changes in the light state of polarization which unavoidably occur in conventional fibers presenting a weak random birefringence [14, 15]. As extensively discussed in ref. [14, 15, 16], those self-oscillations of one-stage RFLs are fully suppressed from an increase of birefringence which can be simply achieved by the use of polarization maintaining fibers (PMFs).

In this paper, we demonstrate for the first time to our knowledge a cascaded RFL in which birth of the second-order Stokes component induces a destabilization of the laser output with the emergence of self-oscillations of the power of all the optical waves. Contrary to conventional one-stage RFLs, we show from our experimental and theoretical study that the observed instabilities do not arise from nonlinear evolution of light state of polarization [14]. We show

#94134 - $15.00 USD Received 20 Mar 2008; revised 5 May 2008; accepted 6 May 2008; published 11 Jul 2008

that they grow from the emergence of a strong second-order Stokes wave which interplays with linearly-polarized pump and first-order Stokes waves via the only stimulated Raman scattering inside a Perot-Fabry cavity. In Sec. 2, we describe our experimental setup which is basically similar to the one presented in ref. [17]. The cascaded RFL considered in our experiments is a grating-free RFL made from a 220−m long highly nonlinear photonic crystal fiber (HN-PCF) [17]. In Sec. 3, we present an experimental study of the dynamical behavior of the grating-free RFL delivering two Stokes components. In Sec. 4, we introduce a simple model incorporating only a few physical ingredients and we show from numerical simulations that it describes qualitatively but also quantitatively well dynamical behaviors experimentally recorded. Sec. 5 is dedicated to a discussion about limitations of our model.

2. Experimental setup

Our experimental setup is schematically shown in Fig. 1. It is basically identical to the setup presented in ref. [17]. The pump source is a linearly-polarized Ytterbium-doped single-mode fiber laser operating at $\lambda_p = 1064$ nm. This laser has a linewidth of ~ 1.3 nm and a maximum cw output power of 20 W. The pump power P_{in} launched inside the fiber can be adjusted by rotating a half-wave plate (HWP1) located before a polarizing cube. The pump power can also be slowly swept by rotating a motorized half-wave plate (HWP2) which is located before the Faraday isolator. The polarization direction of the incident pump field can be rotated with a third half-wave plate (HWP3).

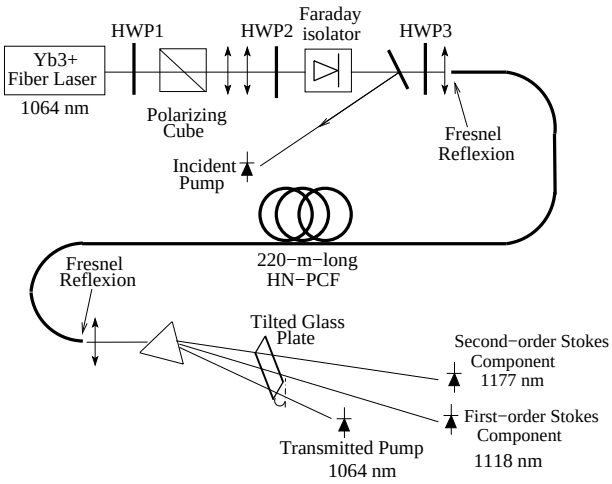

Fig. 1. Schematic representation of the experimental setup.

Our RFL is made from a PCF exhibiting a Raman gain so high that Stokes oscillation can be initiated inside a Perot-Fabry cavity formed only by weak broadband Fresnel reflections from the fiber ends. Briefly summarizing the main characteristics of this grating-free RFL, it consists of a ~ 220 m-long HN-PCF with a geometrical core diameter of ~ 2.5 μm. The HN-PCF has been designed and manufactured by Draka. The germanium content in the doped section of the PCF core is about ~ 25 Wt%, which leads to a Raman gain coefficient G_{R1} as high as ~ 42 km^{-1}. W^{-1} (or $G_{R1} \sim 182$ dB.km^{-1}.W^{-1}) for co-polarized pump and first-order Stokes waves [17]. The Raman gain coefficient G_{R2} giving the coupling strength between the first- and the second-order Stokes components is ~ 38 km^{-1}. W^{-1} (or $G_{R2} \sim 164$ dB.km^{-1}.W^{-1}). Laser oscillation arises from broadband Fresnel reflections of $\sim 3.1\%$ at the PCF cleaved ends. In our grating-free RFL, first-order Stokes emission occurs around $\lambda_1 \sim 1118$ nm at a threshold power

#94134 - $15.00 USD Received 20 Mar 2008; revised 5 May 2008; accepted 6 May 2008; published 11 Jul 2008

P_{Th1} of only $\sim$ 540 mW [17]. The central wavelength λ_2 for second-order Stokes emission is around 1177 nm. Note that the zero dispersion wavelength of the HN-PCF is around 900 nm which means that both pump and Stokes wavelengths are in anomalous dispersion region. The PCF losses measured at λ_p, λ_1 and λ_2 are of $\sim$ 9.6 dB/km, $\sim$ 9.2 dB/km and $\sim$ 8.8 dB/km, respectively.

As shown in Fig. 1, the Stokes beams and the transmitted pump beam are spatially separated in free space by using one prism. A tilted glass plate corrects the anisotropic polarization transmission of the prism. The evolution of total Stokes and pump powers are recorded by two photodiodes which have a 200-MHz bandwidth. These two photodiodes are connected to a 200-MHz digital oscilloscope and a careful calibration procedure allows us to convert their output voltages into optical powers. The relative uncertainty on the measured values of the optical powers, resulting from uncertainty in the calibration procedure, is estimated to be less than $\sim$ 10%. Note that the evolution of the incident pump power is monitored by a photodiode detecting a small amount of light reflected by a glass plate located before the aspheric lens used to launch the light inside the PCF.

3. Laser dynamics

Regarding polarization issues, our grating-free RFL behaves almost as a RFL made with a PMF. As extensively discussed in ref. [17], laser power characteristics are consequently strongly dependent on the polarization direction of the incident pump field. Laser power characteristics shown in Fig. 2 have been obtained by ensuring that polarization direction of the pump and Stokes waves is linearly maintained along one of the PCF birefringence axes. Following a procedure already explained in ref. [17], this has been achieved by minimizing the power threshold of the first-order Stokes component by adjusting the polarization direction of the incident pump field.

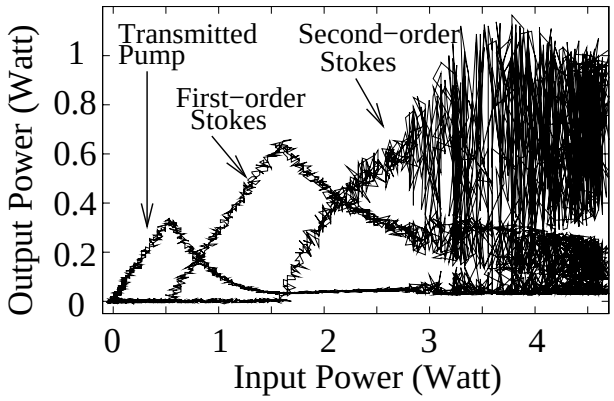

Fig. 2. Characteristics of the linearly-polarized grating-free RFL.

As shown in Fig. 2, the emergence of the second order Stokes component at a power threshold P_{Th2} of $\sim$ 1.6 Watt induces a strong depletion of the power carried by the first-order Stokes wave. On the other hand, the transmitted pump power remains weak and nearly clamped around $\sim$ 40 mW above the threshold of the second-order Stokes wave. The birth of the second-order Stokes wave at a wavelength λ_2 of $\sim$ 1177 nm does not influence the stability of the grating-free RFL as long as the incident pump power does not exceed a threshold power of $\sim$ 2.7 Watt. Above this threshold power, the laser output becomes unstable with self-oscillations of the powers of the three optical waves (see Fig. 2).

#94134 - $15.00 USD Received 20 Mar 2008; revised 5 May 2008; accepted 6 May 2008; published 11 Jul 2008

These self-oscillations have been recorded by fixing the incident pump power at selected values. As shown in Fig. 3, the self-oscillations are periodic with a period of $\sim 1.2\mu$s which is close to the transit time $\tau = nL/c$ of light inside the ~ 220 m-long PCF ($\tau = 1.05\,\mu$s). Whatever the incident pump power, the self-oscillations present a period which is always close to $\tau = nL/c$. This is in drastic contrast with the wide variety of time scales observed at the output of unstable one-stage RFLs. In these RFLs, the time scales characterizing the observed instabilities actually spread out from ~ 0.1 to ~ 50 times the cavity round-trip time [14]. This strong difference between time scales characterizing unstable behaviors in the two types of RFLs is an important feature. It suggests that physical mechanisms responsible from destabilization of cascaded RFLs strongly differ from mechanisms already identified as being responsible from unstable behaviors of one-stage RFLs (i.e. linear and nonlinear changes in the light state of polarization).

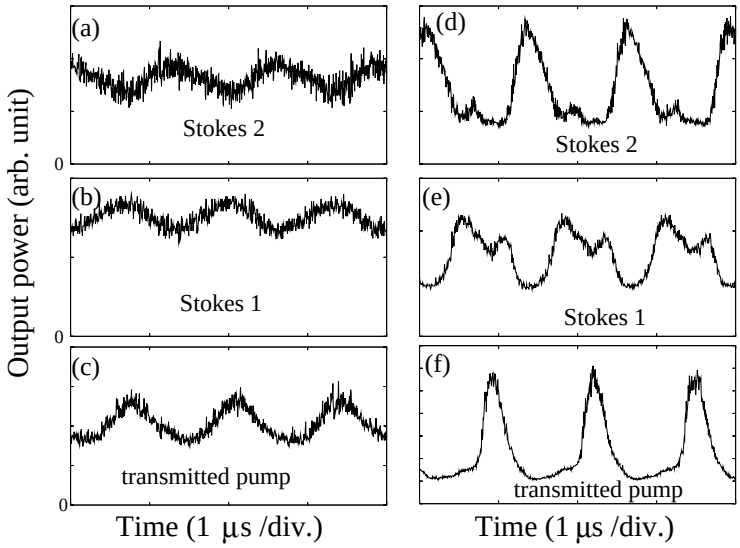

Fig. 3. Self-oscillations experimentally recorded at input pump powers $P_{inc} \sim 3$ W: (a)-(c) and ~ 3.5 W: (d)-(f). Time evolution of the optical power of second-order Stokes wave:(a),(d). Time evolution of the optical power of first-order Stokes wave:(b),(e). Time evolution of the optical power of transmitted pump wave:(c)-(f).

Closely above the bifurcation between the stable steady state and the periodically-oscillating state, we have recorded nearly sine oscillations (see Figs. 3(a)-(c)), which strongly suggests that laser destabilization occurs through a critical Hopf bifurcation. Figures 3(d)-(f) show the self-oscillations recorded at a higher incident pump power of ~ 3.5 Watt. They are strongly distorted from the sine oscillations recorded near the bifurcation point. The occurrence of an antiphase motion between power oscillations of the first- and the second-order Stokes wave represents another important signature characterizing the dynamics of our grating-free RFL. This antiphase dynamics, well evidenced in Figs. 3(a)-(b) and Figs. 3(d)-(e), has been observed whatever incident pump powers exceeding the bifurcation point (i.e. for $P_{in} > 2.7$ Watt). On the contrary no remarkable phase difference is observed between self-oscillations of the transmitted pump wave and the first-order Stokes wave (see Figs. 3(b)-(c) and Figs. 3(e)-(f)). Note that Brillouin fiber ring lasers emitting two Stokes components have been found to present dynamical behaviors qualitatively similar to those observed in our grating-free RFL [18].

#94134 - $15.00 USD Received 20 Mar 2008; revised 5 May 2008; accepted 6 May 2008; published 11 Jul 2008

4. Theoretical analysis

Contrary to dynamical instabilities already reported in conventional RFLs [14], self-oscillations experimentally observed in our linearly-polarized grating-free RFL do not seem to be possibly related to nonlinear evolution of the light state of polarization inside the laser cavity. Experiments show that their birth is associated with the existence of a strong second-order Stokes component interplaying with linearly-polarized pump and first-order Stokes waves inside a low-finesse Perot-Fabry cavity. In the present section, we show theoretically that stimulated Raman scattering is the only physical ingredient which is necessary to describe dynamical behaviors observed in the cascaded RFL. Our way of modeling the cascaded RFL is therefore very different from the approach already used to describe instabilities found in one-stage RFLs. As discussed in ref. [15], unstable behaviors observed in RFLs delivering one Stokes component are actually well described from a model incorporating physical effects influencing the intracavity light state of polarization (i. e. birefringence, optical Kerr effect and stimulated Raman scattering).

In order to understand the origin of instabilities described in Sec. 3, we introduce the simplest dynamical model in which linearly-polarized pump and Stokes waves interplay through the only stimulated Raman scattering inside a Perot-Fabry cavity. Ignoring the influences of optical Kerr effect, fiber birefringence and of group velocity dispersion, partial differential equations governing the spatio-temporal evolution of the various optical powers inside the fiber read [11]:

$$\frac{\partial P}{\partial z}+\frac{n}{c}\frac{\partial P}{\partial t}=-\alpha_p P-G_{R1}\frac{\lambda_1}{\lambda_p}(F_1+B_1)P, \tag{1}$$

$$\frac{\partial F_1}{\partial z}+\frac{n}{c}\frac{\partial F_1}{\partial t}=-\alpha_1 F_1+G_{R1}PF_1-G_{R2}\frac{\lambda_2}{\lambda_1}(F_2+B_2)F_1, \tag{2}$$

$$-\frac{\partial B_1}{\partial z}+\frac{n}{c}\frac{\partial B_1}{\partial t}=-\alpha_1 B_1+G_{R1}PB_1-G_{R2}\frac{\lambda_2}{\lambda_1}(F_2+B_2)B_1, \tag{3}$$

$$\frac{\partial F_2}{\partial z}+\frac{n}{c}\frac{\partial F_2}{\partial t}=-\alpha_2 F_2+G_{R2}(F_1+B_1)F_2, \tag{4}$$

$$-\frac{\partial B_2}{\partial z}+\frac{n}{c}\frac{\partial B_2}{\partial t}=-\alpha_2 B_2+G_{R2}(F_1+B_1)B_2. \tag{5}$$

F_1 (resp. B_1) and F_2 (resp. B_2) represent the optical powers of the first-order and second-order forward-propagating (resp. backward-propagating) Stokes waves. P is the optical power of the forward-propagating pump wave. G_{Ri} ($i=1,2$) are the Raman gain coefficients measured in $\mathrm{m}^{-1}.\mathrm{W}^{-1}$. α_p and α_i ($i=1,2$) are the power attenuation coefficients at pump and Stokes wavelengths, respectively. c/n represents the group velocity of light inside the PCF. As the forward-propagating pump wave is strongly depleted inside the optical fiber, the backward-propagating pump wave reflected at the fiber end is very weak. We have checked from numerical simulations that the backward-propagating pump wave influences the laser power characteristics in a negligible way and we have therefore ignored its influence in our theoretical treatment.

To describe our laser oscillating inside a Perot-Fabry cavity, propagation Eqs. (1)-(5) must be supplemented by the following boundary conditions:

$$P(z=0,t)=P_{inc} \tag{6}$$

$$F_i(z=0,t)=R_{in,i}\ B_i(z=0,t) \tag{7}$$

$$B_i(z=L,t)=R_{out,i}\ F_i(z=L,t) \tag{8}$$

#94134 - $15.00 USD Received 20 Mar 2008; revised 5 May 2008; accepted 6 May 2008; published 11 Jul 2008

where L, $R_{in,i}$ and $R_{out,i}$ represent the PCF length and the power reflectivity coefficients of the cavity at wavelengths λ_i $(i = 1,2)$, respectively. In our experiments, the laser cavity is simply made from from Fresnel reflexions from the fiber ends. In our PCF, the Fresnel reflexion coefficients exhibit a small wavelength dependence so that we simply consider that $R_{in,i} = R_{out,i} = R$ for $i = 1,2$. The transmitted pump power is simply given by $P(z = L,t)$ and output Stokes powers at λ_i $(i = 1,2)$ are given by $(1-R)F_i(z = L,t)$.

We numerically integrate Eqs (1)-(8) by using the so-called method of characteristics [19]. With this numerical scheme, the functions $P(z,t)$, $F_i(z,t)$ and $B_i(z,t)$ $(i = 1,2)$ are spatially discretized inside arrays containing N_{points}. The number of steps needed to compute the time evolution of the output powers over half a round trip is also equal to N_{points}. The order of this numerical method is only of unity and its convergence must be carefully tested by increasing the value of N_{points}. In particular an underestimated value of N_{points} can lead to wrong values of bifurcation points (i.e. laser threshold powers and instabilities threshold power). We have carefully tested those features and the results presented in this paper have been obtained for $N_{points} = 10^4$.

All the numerical simulations have been performed with the measured values of power attenuation coefficients which are given by $\alpha_p = 2.21$ km^{-1}, $\alpha_1 = 2.12$ km^{-1} and $\alpha_2 = 2.03$ km^{-1}. The Raman gain coefficient G_{R1} has been determined in ref. [17] from the measurement of the power threshold of the first-order Stokes component. The value of the Raman gain coefficient G_{R2} has been determined from calculations on the overlap integral between transverse modes and from the germanium doping of the PCF core. Values of G_{R1} and G_{R2} used in numerical simulations are $G_{R1} = 41.9$ km^{-1}W^{-1} and $G_{R2} = 37.8$ km^{-1}W^{-1}, respectively. As in ref. [17], the value of R is taken to 0.03, which is computed from a measured value of the fiber effective index.

As shown in Fig. 4, the first result evidenced in numerical simulations is the occurrence of self-oscillations of the powers of the three optical waves found at the laser output. As in experiments, the period T of the self-oscillations is close to the light transit time $\tau = nL/c$ inside the PCF. More accurately T is equal to 0.92 times the light transit time inside the PCF(i. e. $T = 0.966\mu$s). Numerical simulations evidence phase relations among self-oscillations which are similar to those experimentally observed. In particular, the antiphase motion between the first-order Stokes wave and the second-order Stokes wave is well reproduced by numerical simulations. Finally the shape of time signals numerically computed is also very similar to the shape of experimental signals (compare in particular Figs. 3(d)-(f) with Figs. 5(d)-(f)).

A more complete comparison between experimental and theoretical results is given by the RFL characteristics. As shown in Fig. 5, characteristics numerically computed are very similar to characteristics experimentally recorded (see Fig. 2). The threshold power P_{th2} of the second order Stokes wave measured in experiments ($P_{th2} \sim 1.6$ W) is almost identical to the threshold power obtained from numerical simulations ($P_{th2} = 1.66$ W).

The good agreement between our experimental and theoretical results shows that our model captures the essential of the dynamics of the cascaded RFL. In particular, our analysis shows that only a few physical ingredients, namely coupling between counterpropagating waves via the only stimulated Raman scattering inside a Perot-Fabry cavity, are necessary to describe the laser dynamics in a satisfying way. Although experimental and theoretical results are in good agreement, two slight discrepancies must be noticed. First the threshold for the emergence of the self-oscillations is of 2.2 W in numerical simulations whereas it is of ~ 2.7 W in experiments. Moreover the average output power P_{av} carried by the second-order Stokes wave is lower in experiments ($P_{av} \sim 0.7$ W for $P_{inc} \sim 4$ W, see Fig. 2) than in numerical simulations ($P_{av} \sim 1$ W for $P_{inc} \sim 4$ W, see Fig. 5). The next Section is dedicated to a discussion in which we examine the limitations of our model by describing and considering additional phenomena found in the

#94134 - $15.00 USD Received 20 Mar 2008; revised 5 May 2008; accepted 6 May 2008; published 11 Jul 2008

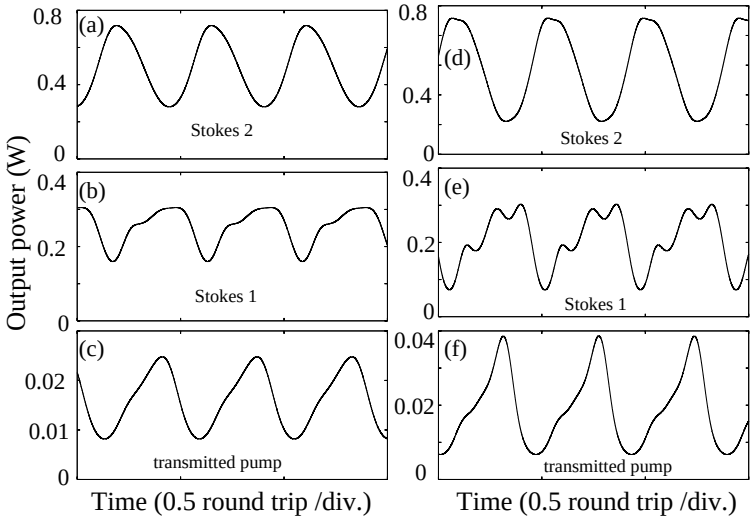

Fig. 4. Numerical simulations : Self-oscillations numerically computed from integration of Eqs. (1)-(8) at incident pump powers $P_{inc} = 2.5$ W: (a)-(c) and $P_{inc} = 2.75$ W: (d)-(f). Time evolution of the optical power of second-order Stokes wave:(a),(d). Time evolution of the optical power of first-order Stokes wave:(b),(e). Time evolution of the optical power of transmitted pump wave: (c)-(f). Parameters used in numerical simulations are: $\alpha_p = 2.21$ km^{-1}, $\alpha_1 = 2.12$ km^{-1}, $\alpha_2 = 2.03$ km^{-1}, $G_{R1} = 41.9$ km^{-1}W^{-1}, $G_{R2} = 37.8$ km^{-1}W^{-1} (*i.e.* $\alpha_p = 9.6$ dB km^{-1}, $\alpha_1 = 9.2$ dB km^{-1}, $\alpha_2 = 8.8$ dB km^{-1}, $G_{R1} = 184$ dB km^{-1}W^{-1}, $G_{R2} = 164.$ dB km^{-1}W^{-1}) , $R = 0.03$, $L = 220$ m, $\lambda_p = 1064$ nm, $\lambda_1 = 1118$ nm and $\lambda_2 = 1177$ nm.

experiments.

5. Discussion

Regarding the input pump power required for the initiation of self-oscillations, we have shown in Sec. 4 that the relative difference between experimental and theoretical values is around $\sim 20\%$. We estimate that this difference is mainly due to the growth of a broadband continuum of light ranging from ~ 1200 nm to ~ 1380 nm. This wide light continuum is evidenced in Fig. 6 which shows the optical spectrum typically measured at the laser output for incident pump powers around ~ 3 W. Increasing the incident pump power, the light continuum continuously grows without any observable threshold effect. Its optical power is negligible for pump powers below the threshold power P_{th2} of the second-order Stokes wave but it increases quickly above this threshold. As an example, for an incident pump power around ~ 2.5 W, it carries a whole optical power of the order of ~ 400 mW when the powers of the first- and second-order Stokes waves are of the order of ~ 300 mW and ~ 500 mW, respectively. Let us emphasize that this broadband continuum is not a third-order Stokes wave. Actually it grows continuously with the first-order Stokes wave and its emergence is not marked by a clear threshold effect, contrary to the two first-order Stokes waves (see Fig. 2). From several secondary experiments, we have noted that the polarization direction of the light continuum is perpendicular to the polarization direction of pump and Stokes waves. Moreover the light continuum is not observed in the backward direction (i. e. the propagation direction opposite to propagation direction of the incident pump wave). The wide light continuum is thus generated in a single pass inside the HN-PCF along a polarization direction perpendicular to the polarization direction of all the

#94134 - $15.00 USD Received 20 Mar 2008; revised 5 May 2008; accepted 6 May 2008; published 11 Jul 2008

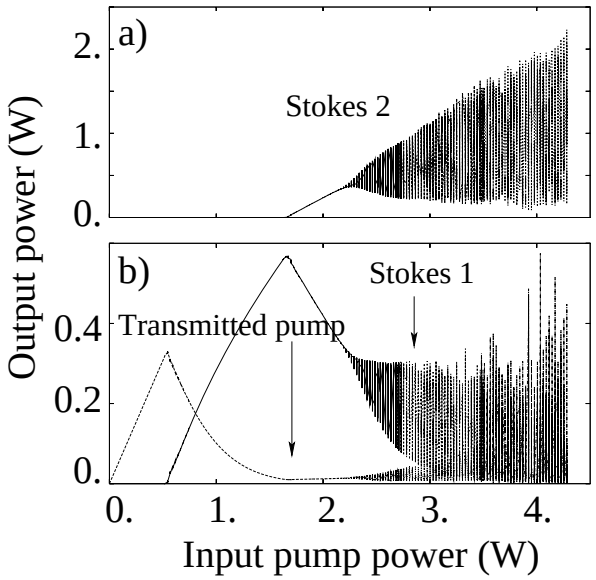

Fig. 5. Numerical simulations : Laser characteristics numerically computed from integration of Eqs. (1)-(8) with parameters identical to those given in the caption of Fig. 4.

waves propagating inside the grating-free RFL. Its exact shape is very sensitive to any weak light feedback inside the HN-PCF. For the moment, we do not clearly understand the origin of the formation of this light continuum but the study of the mechanisms underlying its emergence is itself undoubtedly interesting. It probably arises from the interplay among the various spectral components via stimulated Raman scattering and various cross-phase modulation effects. Anyway the birth of the light continuum can be seen as a loss mechanism responsible from the fact that the power of pump and Stokes waves is less than the one predicted by the simple model presented in Sec. 4. In experiments self-oscillations therefore arise at a pump power higher than the power theoretically predicted.

Let us now briefly explain why a third-order Stokes component is not found at the output of our grating-free RFL at high input pump powers. This additional spectral component should rise at a wavelength λ_3 around 1244 nm. At this wavelength the measured losses of the HN-PCF are as high as ~ 22 dB/km because of OH absorption in this spectral window. The threshold power required to initiate the birth of the third-order Stokes wave is much higher than the maximum pump power that we have been able to launch inside the fiber.

We have used numerical simulations to investigate the origin of self-oscillations observed in experiments. Counterpropagation (i. e. propagation of optical waves in opposite directions) seems to be a key ingredient without which unstable behaviors are no longer observed. Canceling out Raman gain coefficients in equations for backward-propagating optical waves (i. e. setting to zero the functions PB_1 in Eq. (1), B_2F_1 in Eq. (2), PB_1 and F_2B_1 in Eq. (3), B_1F_2 in Eq. (4), and F_1B_2 in Eq. (5)) and keeping all parameters used in Sec. 4 unchanged, all dynamical behaviors described in Sec. 4 vanish and the RFL output is stable. Moreover preliminary numerical simulations show that the finesse of the optical cavity (i.e. fiber linear losses and reflectivity coefficient R) is a parameter that seems to influence the laser stability.

#94134 - $15.00 USD Received 20 Mar 2008; revised 5 May 2008; accepted 6 May 2008; published 11 Jul 2008

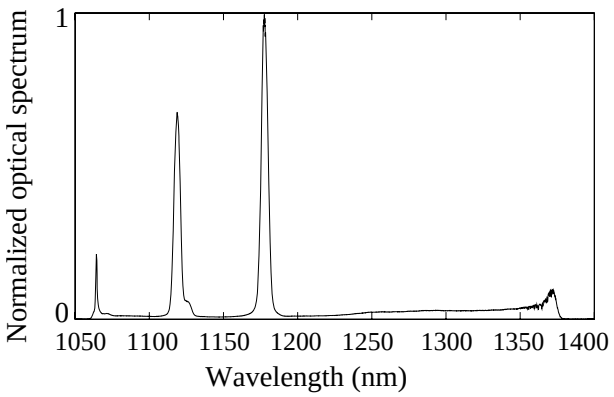

Fig. 6. Typical optical spectrum recorded at the output of the grating-free RFL for input pump powers ranging between ~ 2 W and ~ 4 W.

6. Conclusion

We have reported, for the first time to our knowledge, the observation of self-oscillations of the output power in a cascaded RFL delivering two Stokes components. In our grating-free RFL made with a HN-PCF, the growth of a second-order Stokes wave remaining linearly polarized has been found to deeply influence the stability of the laser output. We have shown that dynamical behaviors experimentally observed are well described by a simple model assuming that linearly-polarized pump and Stokes waves interplay through the only stimulated Raman scattering within a Perot-Fabry cavity. Stimulated Raman scattering is thus identified as being the dominant physical mechanism responsible for the emergence of unstable behaviors inside the Perot-Fabry cavity. This result is in strong contrast with conclusions drawn from previous works about dynamical behaviors found in RFLs emitting a single Stokes component. One-stages RFLs have actually been found to exhibit dynamical instabilities induced by linear and nonlinear physical effects prone to influence the intracavity light state of polarization (i. e. birefringence, optical Kerr effect and stimulated Raman scattering) [14, 15].

The occurrence of self-oscillations at the output of cascaded RFLs is a phenomenon which cannot be ignored by researchers working in the field of design and optimization of cascaded RFLs. Fluctuations of the laser output are actually unacceptable in many applications and the delimitation of their domain of presence is an important problem which deserves further investigations. From a more fundamental point of view, physical mechanisms responsible for laser destabilization must also be further investigated.

Acknowledgements

The Centre d'Etudes et de Recherches Lasers et Applications is supported by the Ministère chargé de la Recherche, the Région Nord/Pas de Calais and the FEDER. This work was supported by the EU framework 6 project "NEXTGENPCF".

#94134 - $15.00 USD Received 20 Mar 2008; revised 5 May 2008; accepted 6 May 2008; published 11 Jul 2008